Materials Chemistry and Physics 124 (2010) 120–128

Contents lists available at ScienceDirect

Materials Chemistry and Physics

journal homepage: www.elsevier.com/locate/matchemphys

Influence of highly branched poly(amido amine) on the properties of hyperbranched polyurethane/clay nanocomposites

Harekrishna Deka, Niranjan Karak*

Advanced Polymer and Nanomaterial Laboratory, Department of Chemical Sciences, Tezpur University, Tezpur 784028, Assam, India

ARTICLE INFO

Article history:
Received 11 March 2010
Received in revised form 1 May 2010
Accepted 2 June 2010

Keywords:
Nanostructures
Polymers
Thermal properties
Thermogravimetric analysis

ABSTRACT

The fascinating architecture of hyperbranched polymer imparts a truck load of novel properties to the material. Epoxy resin modified *Mesua ferrea* L. seed oil based hyperbranched polyurethane (MHBPU) nanocomposites were prepared by *in situ* technique using s-triazine based highly branched poly(amido amine) (HBPAA) modified organo-nanoclay. The HBPAA was synthesized by $A_2 + B_3$ technique with good yield (>75%) using urea and s-triazine. The formation of the polymer was confirmed with the help of ^{1}H NMR, FTIR, UV spectroscopic, and measurements of solution viscosity with other physical properties. This HBPAA was successfully utilized to swell the montmorillonite organo-nanoclay as the interlayer gallery distance increases up to 8.2 Å, obtained by XRD study. The FTIR further confirmed the presence of interactions of the HBPAA moiety with the organo-clay layers. The formation of nanocomposites was confirmed by FTIR, XRD, SEM, TEM and rheological studies. The improvements of tensile strength (1.7 times) and scratch hardness (2.3 times) along with the dramatic enhancement of thermostability and flame retardancy without compromising impact resistance, bending, and elongation at break of the nanocomposites compared to pristine MHBPU thermoset are the noticeable credits of the present investigation. The results signify the great potential of the studied materials for various advanced applications.

1. Introduction

Polymer/clay nanocomposite (PCN) is one of the hottest research topics in the domain of material science over the last two decades for its fascinating properties [1]. Typically, on incorporation of ≤5 wt% clay leads to the significant improvement in performance of the matrix. The improvements in mechanical properties, flame retardancy, thermostability, gas barrier properties are noticeable after nanocomposite formation [1,2]. The high surface to volume ratio and easy intercalation ability of nanoclay account for such enhancements of the properties compared to that of the conventional composites [3]. The polymer chain dynamics are highly altered due to the restricted conformational degree of freedom of chains as imposed by the clay platelets. As a result, the polymer chains form a large volume fraction of the nanocomposite in the nano-confined environment and the overall properties are influenced in an unusual manner [4]. There has been considerable and rising interest in the study of PCN, especially with montmorillonite (MMT) nanoclay. The lamellar structure of MMT provides high stiffness and high aspect ratio (100–1000) along with high swellability and ease of surface modification either by chemical or physical means [5]. The property optimization of the nanocomposites depends on dispersion state of fillers, particles packing or alignment and the ability to transfer interfacial stress [6] from polymer to filler. On the other hand, these factors depend on the ease of polymer chain intercalation into the interlayer galleries of MMT and thus modification of MMT plays the major role in tuning the desired properties of PCNs. Therefore it has been a common practice to render the hydrophobicity to the hydrophilic clay before nanocomposite formation. Alkylammonium and alkylphosphonium are widely used to modify MMT clay in order to achieve exfoliated structure of the nanocomposites [7]. These organic cations lower the surface energy of clay and enhance the wettability of clay with polymer. For further enhancement of the properties of PCNs, the alternate functional modifiers are also being used [8]. Lot of reports on polymer/modified MMT nanocomposites described the use of different type of amine for MMT modifications [9,10]. These include aliphatic primary, tertiary, quaternary amines and oligomeric amine derivatives. In all the modification processes, it has been observed that the nature of amine compounds, length of alkyl chain etc. depict the ultimate properties of the nanocomposites. Xiong et al. described the improvement of thermal stability and modulus of the aromatic amine modified MMT/polyurethane (PU) nanocomposites [11]. Recently Bhowmick and co-workers reported distinctive differences between the properties of modified MMT/PU nanocomposite and unmodified MMT/PU nanocomposites [6]. They observed improvement in tensile strength, thermal stability, storage modulus and adhesive properties of the modified

* Corresponding author. Tel.: +91 3712 267209x5056; fax: +91 3712 267006.
E-mail address: karakniranjan@yahoo.com (N. Karak).

0254-0584/$ – see front matter © 2010 Elsevier B.V. All rights reserved.
doi:10.1016/j.matchemphys.2010.06.002

clay nanocomposites over the pristine PU. It is to be worth note that though a plethora of reports described the effect of different type of amine on MMT modification, the influence of insertion of s-triazine based highly branched amine into the MMT gallery is not studied, till now. The s-triazine based highly branched polymers are known for their interesting physical, chemical and thermal properties [12,13]. Therefore it is expected that the incorporation of such moiety into the MMT layers and their nanocomposites would certainly lead to the genesis of high performance materials.

Further a wide attention is being paid to the PU chemistry for its unique properties and versatile applications. The excellent abrasion resistance, inherent high mechanical strength, tear strength, ease in processing, flexibility and elasticity of PU augment its demand while certain limitations like inadequate thermal stability and flame retardancy restrict its end uses in certain areas [14]. The formation of PU/clay nanocomposites may eliminate the above drawbacks and thus attempt has been made to investigate the same in the present study. Further, like other hyperbranched polymers, hyperbranched polyurethanes (HBPUs) have also drawn a great deal of attention due to their unique architectural features such as non-entangled three dimensional structures, low melt and solution viscosity, good solubility and large number of terminal functional groups. Again, bio-based hyperbranched polymers bring one step ahead from the green chemistry point of view. The present investigation utilized the epoxy modified *Mesua ferrea* L. seed oil, a renewable resource, based hyperbranched polyurethane system (MHBPU) as the matrix [15].

Herein authors wish to report the effect of insertion of the s-triazine based highly branched poly(amido amine) (HBPAA) in organo montmorillonite (OMMT) clay layers and on MHBPU/clay nanocomposites. The characterization and property evaluation of MHBPU/modified OMMT nanocomposites are also described here. This article primarily focuses on the mode of modification and its effect on the properties of MHBPU/modified OMMT nanocomposites.

2. Experimental

2.1. Materials

The *M. ferrea* L. seeds (about 70% oil content) were collected from Darrang, Assam. The seed oil was isolated by solvent soaking method and purified by alkali refining technique. Using standard glycerolysis procedure monoglyceride of the oil was prepared. Diisopropyl ethylamine (DIPEA, Merck, India), lead monoxide (S.D. Fine Chemical Ltd., India) and 2,4-toluene diisocyanate (TDI, Sigma Aldrich, Germany) were used as received. Glycerol (Merck, India) and poly(ε-caprolactone) diol (PCL, Solvay Co., UK, M_n = 3000 g mol^{-1}) were dried before use. 2,4,6-Trichloro-1,3,5-triazine (CYC, Sigma Aldrich, Germany) and urea (Merck, India) were used after purification by recrystallization. N,N′-dimethylacetamide (DMAc) and N,N′-dimethylformamide (DMF) of Merck, India was purified by vacuum distilled over calcium oxide and kept in 4A type molecular sieves. Octadecylamine-modified nanoclay (OMMT) was obtained from Sigma Aldrich, Germany. Bisphenol-A based epoxy resin (CY 250) and poly(amido amine) hardener (HY 840) (Ciba Geigy, India) were used as supplied. Other reagents are reagent grade and used without further purification unless otherwise stated.

2.2. Synthesis of highly branched poly(amido amine)

Synthesis of the HBPAA was carried out by the following method. A three neck round bottom flask was purged by N_2 gas. 1.80 g (0.03 mol) of urea and 2.59 g (0.02 mol) of DIPEA in 90 mL DMAc were taken in the flask. Then 3.69 g (0.02 mol) of CYC solution in 35 mL DMAc was added drop wise for 0.5 h at 0 °C with constant stirring. The reaction mixture was stirred for 2 h at 0–5 °C, followed by 2 h at 30–35 °C after adding 2.59 g of DIPEA and 2 h at 80 °C with further 2.59 g of DIPEA. The reaction was finally continued for another 2 h at 100 °C. It was then cooled and poured slowly with constant stirring in CH_2Cl_2. The precipitate formed was separated by filtration and washed several times with water, methanol followed by acetone to remove the unreacted reagents. The collected product was dried under vacuum at temperature 40 °C for 24 h to get the dry powder.

2.3. Preparation of hyperbranched polyurethane and its modification

The details of the preparation process of the HBPU were described elsewhere [16]. Firstly, a pre-polymer was prepared from 2 mol of PCL, 3 mol of monoglyceride of *M. ferrea* L. seed oil and 7.5 mol of TDI. Finally, the polymer was synthesized by the reaction of the pre-polymer with 2.5 mol of glycerol. The prepared HBPU was obtained in DMF as a solution of 25–30% solid content (w/v).

Further the HBPU was modified by commercially available epoxy resin and poly(amido amine) hardener to improve its performance characteristics. This modified HBPU/epoxy system (MHBPU) was used as the matrix for the preparation of the nanocomposites. The modification process was described in details somewhere else [15]. In short, the HBPU was mixed with 20 wt% (with respect to HBPU) of epoxy resin (100% solid content) and poly(amido amine) hardener (25% by weight with respect to the epoxy resin) at room temperature (ca. 25 °C) by mechanical stirrer.

2.4. Modification of clay by HBPAA

Two different methods were adopted to modify the OMMT. In one of the way, 1 g of the synthesized HBPAA was dissolved in 5 mL of DMF and mixed with a solution of OMMT (2 g) in 10 mL of DMF. The mixture was vigorously stirred for 4 h and finally sonicated for 15 min. A part of the modified clay was then dried at 80 °C for further study. In another method, 1 g of HBPAA was dissolved in 20 mL mixture of ethanol and HCl (10:1, v/v) and refluxed for 1 h. Then 2 g of OMMT was added to the above mixture and refluxed for another 6 h. Then, the mixture was filtered and washed repeatedly with hot water for complete removal of Cl^- ions (as no precipitate was observed on addition of the 0.1 M $AgNO_3$). The modified clay was then dried under vacuum at 80 °C.

2.5. Nanocomposites preparation

The MHBPU nanocomposites with the modified OMMT were prepared by *in situ* technique. Requisite amount of the modified dispersed clay (1, 2.5 and 5 wt%) in DMF was added into the pre-polymer, obtained by the aforestated procedure. The protocol was the same up to MHBPU preparation. Ultrasonicator (UP200S, Heishler, Germany) was used at various amplitude and half cycle for different time period for homogenization of the mixtures. Finally, the nanocomposite films were prepared by solution casting followed by vacuum degassing and curing at 120 °C for specific time for further testing and analysis. The cured films were denoted as MHBPUMNC1, MHBPUMNC2.5 and MHBPUMNC5 correspond to the modified clay content of 1, 2.5 and 5 wt% respectively by sonication and MHBPUMNC2.5 (E) correspond to the modified clay of 2.5 wt% by exchange process. The nanocomposite with 2.5 wt% OMMT only was denoted as MHBPUNC2.5 as reported earlier [17].

2.6. Analysis and characterization techniques

The FTIR spectra were record by Impact 410, Nicolet, USA spectrophotometer using KBr pellets. ^{1}H NMR spectrum of the HBPAA was recorded by a 400 MHz, Varian, USA spectrometer using d_6-DMSO as the solvent and TMS as the internal standard. The inherent viscosity of the HBPAA was measured with 0.5% (w/v) of polymer solution in DMSO at 25 ± 0.1 °C with the help of Ubbelohde suspended level viscometer. Size and distribution of the clay layers were studied using transmission electron microscope (TEM) JEM 2100, JEOL, Japan at operating voltage of 200 kV. The surface morphology of the nanocomposites was observed by scanning electron microscope (SEM) of model JSM-6390LV, JEOL, Japan. The surface of the sample was platinum coated before SEM analysis. The rheological studies were done with the help of rheometer (CVO100, Malvern, UK). Thermal degradation study was carried out by thermogravimetric analysis, TGA (TG 50, Simadzu, Japan) from 25 °C to 650 °at a heating rate of 10 °C min^{-1} under the nitrogen flow rate of 30 mL min^{-1}. The differential scanning calorimetry (DSC) was done by DSC 60, Simadzu, Japan at 3 °C min^{-1} heating rate with the nitrogen flow rate of 30 mL min^{-1} from −50 to 100 °. The X-ray diffraction (XRD) study was performed at room temperature (ca. 25 °) on a Rigaku X-ray diffractometer, UK over the range of 2θ = (1–30)°. The mechanical properties such as tensile strength and elongation at break were measured by universal testing machine, UTM, of model Z010, Zwick, Germany with a 10 kN load cell and crosshead speed of 20 mm min^{-1}. The casted nanocomposite sheets (∼1 mm thickness) were cut by the manual sample cutter with dimension as per the ASTM D 412-51T for mechanical testing. The measurement of specific gravity, impact resistance, hardness and flexibility (bending) tests was performed according to the standard methods [17]. The flame retardancy of the nanocomposites was tested by measurement of limiting oxygen index (LOI) value by flammability tester as per the ASTM D 2863-77 method. UL 94 test method was also used to measure the flame retardancy of the nanocomposites [18]. The samples were cut into pieces of size 10 in. × 3 in. × 0.035 in. and were mounted vertically in such a way that the gap between the specimen and the surgical cotton placed directly below the specimen was 12 in. in this technique. A flame was then applied to the center of the lower edge of each specimen at an angle of 45° for 10 s. A total of five tests were done for each specimen.

2.7. Sample preparation for mechanical properties

The polymer nanocomposite solutions were applied on mild steel strips ($150 \times 100 \times 1.44\,mm^3$) for impact resistance and scratch hardness studies. Similarly, tin strips ($150 \times 50 \times 0.19\,mm^3$) were coated for bending test. All the films were found to be in the range of 60–70 μm thick as measured by a Pentest coating-thickness gauge (Model 1117, Sheen Instrument Ltd., UK).

3. Results and discussion

3.1. Synthesis and characterization of HBPAA

The s-triazine based HBPAA was synthesized by $A_2 + B_3$ technique using urea (as A_2) and CYC (as B_3) for the first time. Both the CYC and urea are very common and readily available chemicals. They undergo nucleophilic displacement polymerization reaction under appropriate conditions. The polycondensation reaction was carried out at three different temperature rang as the reactivity of the three chlorine atoms of CYC was different [12]. The highest reactivity is assigned to the first chlorine atom of the triazine moiety followed by the second chlorine atom, while the last one possesses the lowest reactivity for the passivation effect of amine substituent. Thus in this stage wise polycondensation reaction, the first chlorine atom has been substituted at 0–5 °C, the second one substituted at 30–35 °C and the third at 95–100 °. Further this stage wise fashion helped to prevent the gel formation. As it may be a problem in such synthesis. The 12% (w/v) CYC solution was slowly added to the urea solution of the same concentration in DMAc solvent and the mole ratio of A_2:B_3 was maintained at 3:2. The HCl gas, formed during the polymerization process, was trapped by using DIPEA as the scavenger. This promoted the reaction toward forward direction.

The HBPAA are soluble in highly polar solvents like DMSO, DMF, NMP, DMAc and partially soluble in THF. Also it is soluble in acids like dilute aqueous HCl, acetic acid etc. The large number of surface amine groups and globular structure of the hyperbranched polymer render them high solubility. The density of the synthesized polymer was found to be $1.31\,g\,cm^{-3}$, and it was light brown in color. The presence of rigid aromatic moiety and hydrogen bonding (confirmed from FTIR) leads to this moderate density value. The XRD study revealed the amorphous nature of the polymer. This is the highly branched structure of the polymer that prevent from compactness. The inherent viscosity was found to $0.18\,dL\,g^{-1}$. The non-entangled chain segments render it low solution viscosity.

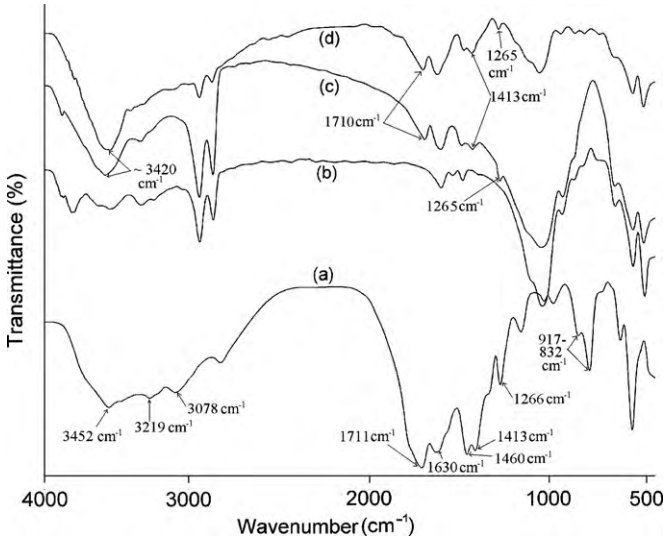

Fig. 1. FTIR spectra of (a) HBPAA, (b) OMMT, (c) modified OMMT (sonicated) and (d) modified OMMT (exchanged).

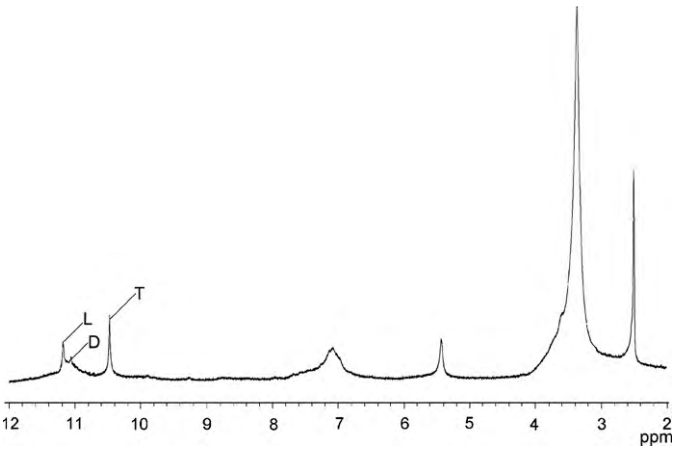

Fig. 2. ^{1}H NMR spectrum of HBPAA (T = terminal, L = linear and D = dendritic unit).

The λ_{max} of the HBPAA in DMAc solvent was found to be 340 nm. This indicates the presence of aromatic structure with conjugation. The FTIR spectrum of the HBPAA is given in Fig. 1(a). The bands at 3452 and 3219 cm^{-1} are the coupling N–H stretching vibration of the primary amine. The band at 3078 cm^{-1} corresponds to the N–H stretching vibration of the secondary amine [19]. The bands at 1711 and 1630 cm^{-1} are for C–N (Amide III band) and C=O stretching frequency of amide respectively. The N–H bending vibrations for primary amine were observed at 1460 cm^{-1} while this band for secondary amine was enveloped by the C=O stretching frequency. The N–H wagging bands for both the primary and secondary amine were seen at 917–832 cm^{-1} region [19]. The presence of the triazine moiety in the hyperbranched structure can be confirmed from the bands at 1413 cm^{-1} (C=N stretching vibration) and 1266 cm^{-1} (aromatic C–N stretching vibration). The ^{1}H NMR study (Fig. 2) further confirmed the formation of hyperbranched structure as it indicates the presence of different types of protons. The occurrence of three different units viz. dendritic, terminal and linear was confirmed from the three peaks of the secondary –N–H protons of the hyperbranched polymer. The peak at $\delta = 10.5$ ppm is due to the –N–H protons attached with the terminal unit. While the peak at $\delta = 11.3$ ppm corresponds to the –N–H protons attached with the linear unit and the peak at $\delta = 11.1$ ppm appears for the –N–H of the dendritic unit. The $-NH_2$ protons are observed at $\delta = 2.5$ ppm. A broad signal around $\delta = 5.2$ ppm corresponds to the amide –NH proton. The peak around $\delta = 3.6$ ppm is due to the DMSO solvent [20]. Degree of branching (DB) of hyperbranched polymers is the scale of structural perfection and it is often determined by the Frechet's equation [21] as:

$$DB = \frac{D + T}{D + T + L} \quad (1)$$

where, D, T and L are the number of dendritic, terminal and linear units in the structure of the hyperbranched polymer respectively. Here, the DB was experimentally determined from the integration of the peak of the respective units in the ^{1}H NMR spectroscopy. And it was found to be 0.52. The DB for linear polymer is close to zero, for hyperbranched polymer it is 0.5 and for dendrimers this value is 1.0. Thus the obtained value indicates the highly branched structure of the prepared polymer.

3.2. Modification of nanoclay

The XRD diffraction patterns of OMMT and modified OMMT (both by sonicated and exchange processes) are shown in Fig. 3. The characteristic diffraction peak appeared at $2\theta = 4.17°$, 3.01° and 3.31° for OMMT, modified OMMT (sonicated) and modified OMMT

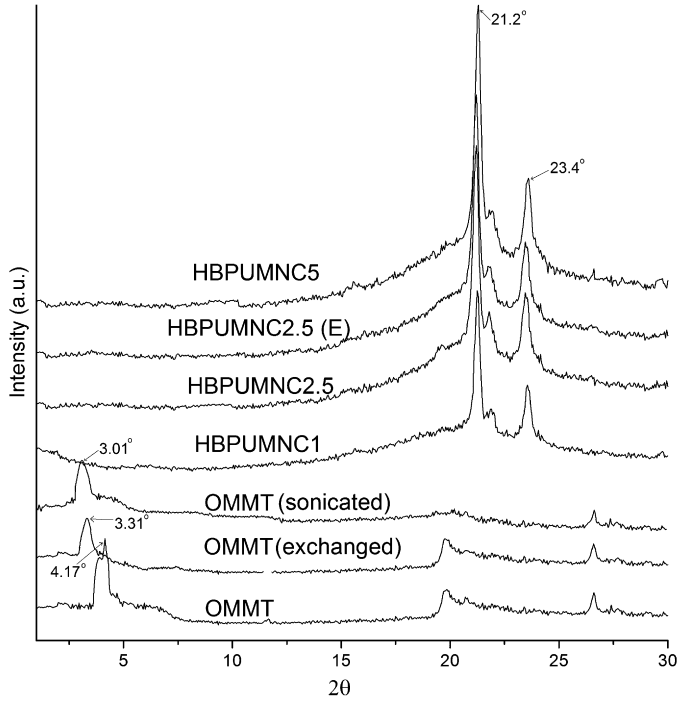

Fig. 3. XRD diffractograms of (a) OMMT, (b) modified OMMT (sonicated), (c) modified OMMT (exchanged), (d) MHBPUMNC1, (e) MHBPUMNC2.5 and (f) MHBPUMNC5.

(exchanged) respectively. Thus the basal spacing increases from 2.11 nm to 2.93 nm in modified OMMT (sonicated) and 2.66 nm in modified OMMT (exchanged) as calculated from Bragg's Equation. The sonication has a prominent effect on modification of the nanoclay through forming efficient acoustic cavitations [22]. It was observed that the peaks were broaden and less intense than the original peak. This reveals increase of disorder of the clay layers [23]. This is due to the non-entangled structure of HBPAA that failed to open up the layers to a greater extent compared to the oligomeric diamine. But at the same time due to their globular shape, the ease of insertion into the clay galleries increases and the high surface functionality provides sites for interactions with clay and matrix. Several literatures described the insertion of polymer chain with

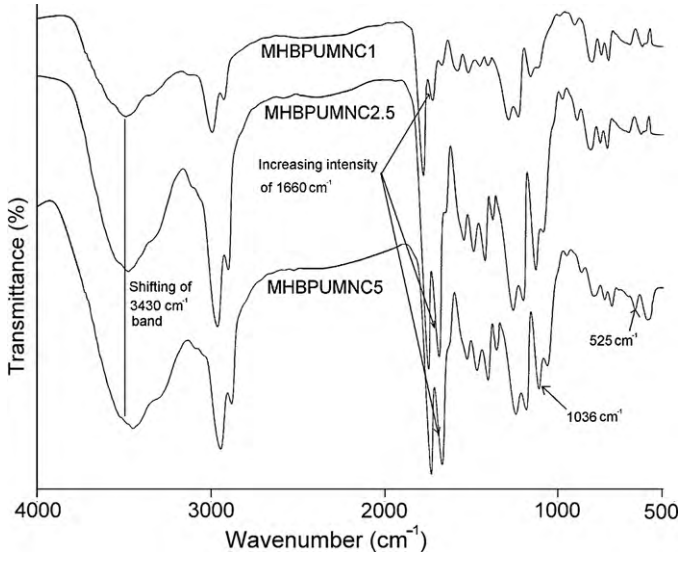

Fig. 4. FTIR spectra of the nanocomposites.

molecular weight higher than 2000 g mol^{-1} and resulted an increment of gallery distance up to 8 Å [9]. Here in this investigation this value 8.2 Å. Helical conformation or double layer planar zigzag disposition models are used to explain such phenomena [24]. This opening up of clay layers helped in ease of insertion of HBPU chain into the galleries. At the same time the surface end groups may provide more wetting capacity of the HBPU to the clay through formation of physical such as hydrogen bonding, polar-polar interactions etc. as well as chemical bond formation compared to the linear systems.

The FTIR spectra of the OMMT and modified OMMT (both sonicated and exchanged) are shown in Fig. 1. The broadening of the bands ~3420 cm^{-1} is the consequence of overlapping of –O–H and –N–H vibration bands of primary and secondary amines [25]. The appearance of the new bands at 1710, 1413 and 1265 cm^{-1} in the modified OMMT spectra correspond to the presence of –C=O of amide, C=N stretching vibration of triazine moiety and aromatic C–N stretching vibration in the clay layers. The marginal shift of the bands in comparison with the pure HBPAA spectrum (Fig. 1) is due to the formation of hydrogen bonding amongst surface amine to the hydroxyl groups of the clay.

3.3. Characterization of the nanocomposites

One of the interesting results was observed in curing study. One of the most interesting results was observed in curing study of the present systems. While in our previous report the nanocomposite MHBPUNC2.5 needed 45 min [17], the present nanocomposite, MHBPUMNC2.5 took only 30 min for complete curing. It was also noticed that with the increase of clay content the time required for curing was reduced. This may be due to the increase in amount of amine groups that are contributed to the curing of the systems.

The primary investigation of formation of the nanocomposites was done by XRD analysis (Fig. 3). The diffraction peak for d_{001} plane of the clay that appeared at $2\theta = 3.01^\circ$ diminished in the nanocomposites. This absence of Bragg scattering is the indication of delamination of the clay tactoids as the disappearance is not due to the limitation of the instrument since the concentration of clay in the matrix is in the range of detection and also there is no heavy element present in the systems. The squeezing tendency [25] of the clay in the nanocomposites that resulted the intercalated structure was prevented by the HBPAA. Also the incorporation of the HBPAA facilitates the compatibilizing ability of the MHBPU matrix to the clay by formation of different types of interactions such as hydrogen bonding, polar-polar interactions etc. These interactions through bridge, loop and tail linkages of the polymer chains (shown in Scheme 1) with the clay layers contributed to the formation of well dispersed clay layers. It is worth to note that the two peaks observed for the modified thermoset matrix at $2\theta = 21.2^\circ$ and 23.4° are due to the d_{110} and d_{200} plane of PCL moiety [26] remain unaltered after nanocomposite formation. However, increment in the intensity of the two peaks can be seen from Fig. 3. The enhancement in the crystallinity might result in the increment in intensity that is explained later on by DSC results.

The FTIR spectra of the nanocomposites are given in Fig. 4. The increase of hydrogen bonding with the incorporation of the polar bonds like urethane, epoxy etc. was the reason of shifting the band from 3420 cm^{-1} to 3430 cm^{-1}. With the increase of clay content this shifting was more as seen from Fig. 4. Such behavior is also supported by other literatures [27]. The increase of intensity of the band 1666 cm^{-1} is due to the increase of –C=O of amide linkages with the increase of clay content. The appearance of the characteristic bands at 525 and 1036 cm^{-1} corresponding Al–O and Si–O–Si stretching vibration that confirms the presence of nanoclay in the systems [17]. Although the dispersion state of the nanoclay cannot

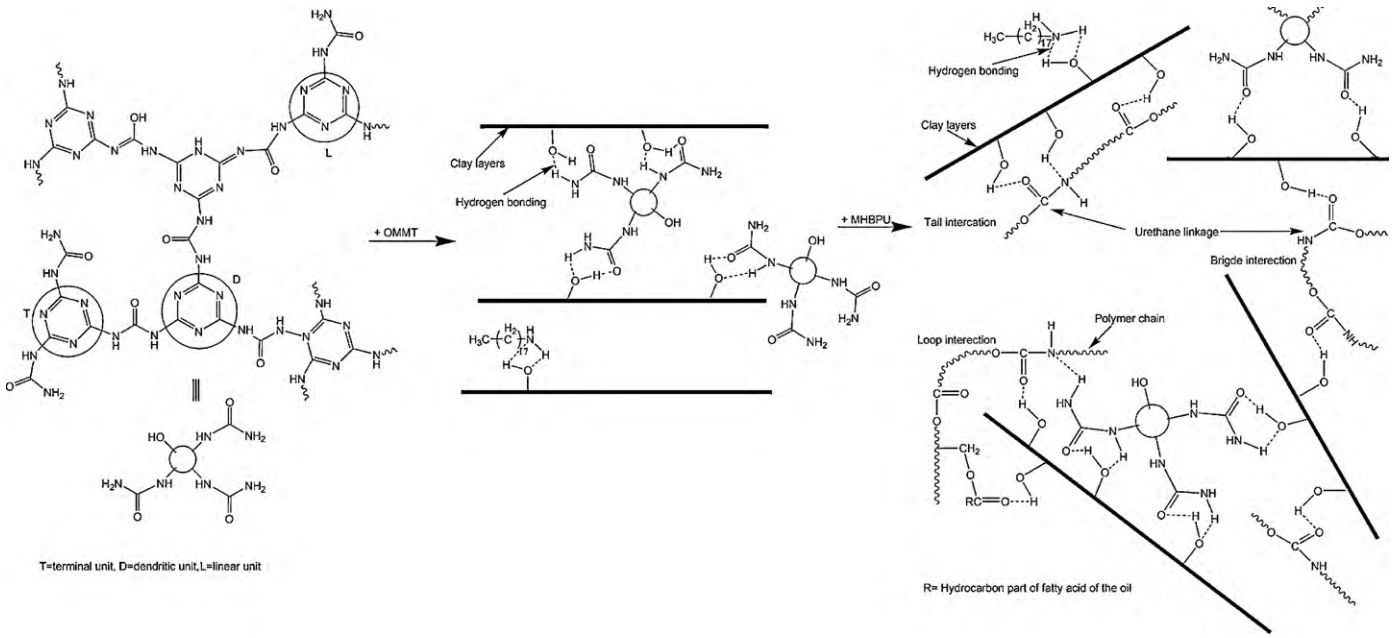

Scheme 1. Possible interactions in the nanocomposites.

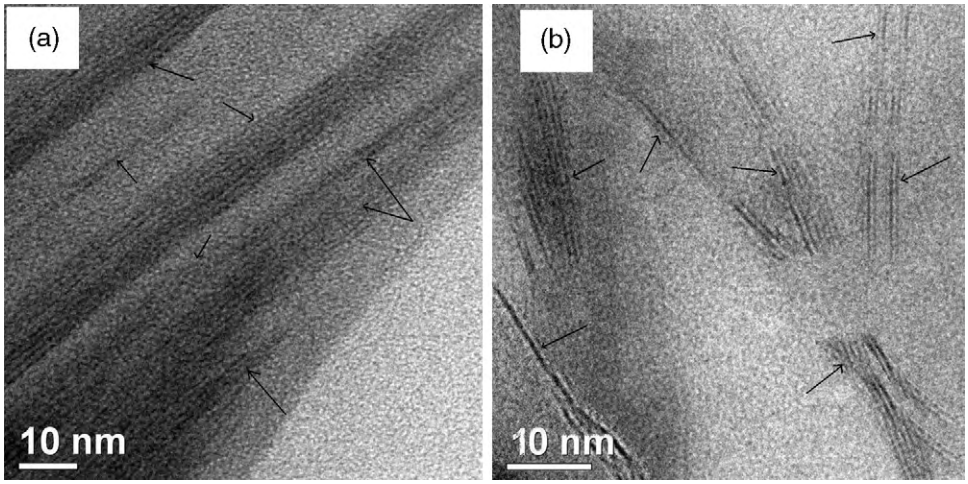

Fig. 5. Representative TEM images of (a) MHBPUMNC1 and (b) MHBPUMNC5.

be obtained from FTIR spectra directly, still the indistinguishable spectra that were taken haphazardly from the nanocomposites convinced to state that the modified OMMTs were uniformly dispersed in the MHBPU matrix. To support the XRD results and to visualize the state of dispersion of the clay platelets in the matrix, the representative TEM micrographs of MHBPUMNC1 and MHBPUMNC5 are shown in Fig. 5.

The TEM images disclose the actual picture what are happening inside the matrix. Fig. 5 reveals the dispersed and disordered clay layers in the matrix. The well dispersed clay layers are indicated by the arrow marks. Thus exfoliated structure of the clay in the MHBPU matrix can be seen from the TEM images. This exfoliation of the clay layers was achieved due to the combined action of mechanical shearing and sonication, which increase the inter-

Table 1
Mechanical properties, LOI values and UL 94 rating of MHBPU matrix and the nanocomposites.

	MHBPU[a]	MHBPUNC2.5[b]	MHBPUMNC1	MHBPUMNC2.5 (E)	MHBPUMNC2.5	MHBPUMNC5
Tensile Strength (MPa)	31.2	46.6	42.0	46.1	48.2	51.4
Elongation at break (%)	512	450	460	432	430	422
Impact resistance (cm)	92	97.7	>100	97	>100	>100
Bending (di. mm)	<5	<5	<5	<5	<5	<5
Scratch Hardness (Kg)	4.3	9.3	8.7	9.4	9.1	9.8
UL94	V2	V2	V1	V1	V1	V1
LOI value	27	28	30	32	33	36

[a] Ref. [15].
[b] Ref. [17].

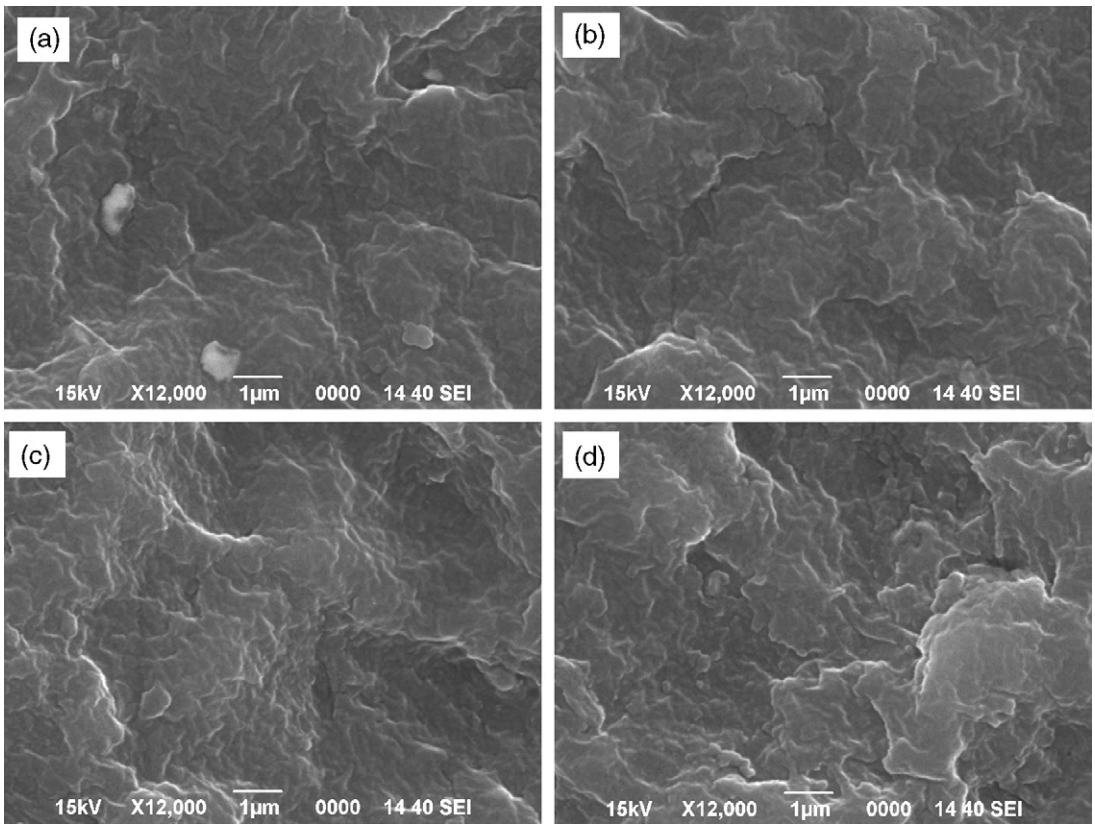

Fig. 6. SEM images of (a) MHBPUMNC1, (b) MHBPUMNC2.5, (c) MHBPUMNC2.5 (E) and (d) MHBPUMNC5.

actions between clay and matrix (as proved by the FTIR study). Further, these interactions are attributed to the proper modification of the OMMT by HBPAA. These uniform dispersion of the clay layers is the reason for the disappearance of the diffraction peak at $2\theta = 3.01^\circ$ in the XRD diffractograms. Nonetheless it is appropriate to state here that while the TEM images give local microscopic information, XRD analysis provides the macroscopic facts.

SEM is also valuable technique for examining the morphology of the system. The SEM images of the fractured surface of the nanocomposites are given in Fig. 6. The bumpy surface showed the uniform distribution of the clay layers. No aggregation or agglomerization was observed in the micrographs which support the TEM observations.

3.4. Rheological study

The rheological properties of PCNs depend on the dispersion state of clay in the matrix and the strength of the polymer–clay interactions [28]. The storage modulus (G'), loss modulus (G'') and complex viscosity (η^*) of the nanocomposites in their melt state are shown in Fig. 7. The test was carried out at 120 °C with varying frequency from 1 to 100 Hz. All the nanocomposites showed apparent plateau for both G' and G'' at low frequencies (Fig. 7(a and b)). The formation of the percolated structure of anisotropic tactoids of clay platelets in the sluggish state or the intra frictional interactions amongst the anisotropic clay tactoids might be the cause of this pseudosolid-like behavior of the nanocomposites at low frequencies [29]. The enhanced moduli also account the increased mechanical properties (discussed later) of the nanocomposites. The η^* values were high in the low frequency region (Fig. 7(c)) and decreased in high frequency region. Thus oscillation-thinning behavior was observed for all the nanocomposites. The homogeneous dispersion of the nanoclay patronized the retarded relaxation in terms of the frictional interactions between the clay tactoids and increased the complex viscosity at low frequencies. However, at high frequency region the frictional interactions fail to resist the flow of the molten nanocomposites due to the large changes in the matrix mobility. This enhanced mobility in high frequency attributed to the effect of physical contacts between the nanoparticles and the matrix and hence decreases the complex viscosity.

3.5. Mechanical properties of the nanocomposites

The effect of clay modification and concentration of the modified OMMT on the mechanical properties was elucidated in the Table 1.

Table 2
Thermal properties of the nanocomposites and pristine polymer.

	MHBPU[a]	MHBPUNC2.5[b]	MHBPUMNC1	MHBPUMNC2.5 (E)	MHBPUMNC2.5	MHBPUMNC5
T_{on} (°C)	240	349	357	359	363	371
T_{max} (°C)	350	402	417	418	423	430
T_m (°C)	50	54	54	55	56	58
ΔH_m (J g^{-1})	53.7	55.8	56.2	57.0	58.2	61.2

[a] Ref. [15].
[b] Ref. [17].

In the nanocomposites, the high aspect ratio of the nanofillers develops unique interactions with the polymer chains and that give rise to optimal control of mechanical properties. It was observed that with the increased of clay the tensile strength increases and a maximum up to 1.7 times increment was achieved. The improvement of tensile strength of the modified clay nanocomposites is well supported by various reports [30]. Due to the high aspect ratio and large surface area, the clay nanocomposites showed improved modulus of elasticity [11]. Further the crystallinity of semi-crystalline polymer matrix can be altered by the presence of nanofillers. In this study the enhancement of crystallinity of the nanocomposites (as observed from the XRD and DSC study) in the presence of clay may also contributes to the improvement of mechanical properties. The inter layer distance of the clay increases due to the modification of clay by the HBPAA. This helps in incorporation of more amount of HBPU chain into the clay tactoids. The degree of enlargement of clay layers consequently increases the effective filler volume fraction and hence polymer stiffness [31]. Also, the interface interactions in between the clay and polymer matrix increased due to the presence of more functional groups after modification. These enhanced physico-chemical interactions result more wetting capability of the matrix (Scheme 1). Thus the applied stress can be effectively transferred to the nanoclay. On the other hand, the increased stiffness reduces the elongation at break value of the nanocomposites (Table 1). The restricted motion of the polymer chains is the reason of this decrement. Nonetheless the flexible PCL and long fatty acid chain of the *M. ferrea* L. seed oil assist the deformation to a certain extent and thus the decrement was not so high [17]. The nanocomposites showed enhanced impact resistance and scratch hardness compared to the pristine matrix and MHBPUNC2.5 (Table 1). The uniform distribution of the nanoclay helped to absorb the applied energy throughout the matrix. The overall enhancement of the tensile strength of these flexible films is one of the factors attributed to these increments. The nanocomposites were flexible enough to bend the films up to 5 mm parallel mandrel without any damage. This retention of flexibility is one of the interesting results achieved. The long fatty acid chain of the *M. ferrea* L. seed oil and PCL moiety conferred this flexibility.

3.6. Thermal properties of the nanocomposites

The thermostability of the nanocomposites was determined by TGA (Fig. 8). It is evident that the degradation temperature of the matrix increased after nanocomposite formation. The well dispersed nanoclay layers are acting as the physical barrier to the decomposed products for escaping from the matrix. Thus the volatile products have to come across a torturous path way during thermal decomposition. Further the thermal motion of the polymer chains was quite reduced by the increased in interfacial interactions between the clay and the matrix. This also helped in the improvement of thermal stability. The characteristic thermal decomposition temperatures such as initial decomposition temperature (T_{on}), temperature corresponding maximum rate of weight loss (T_{max}) are shown in the Table 2. The decomposition temperature was improved by 128 °C for MHBPUMNC5 compared to MHBPU. The thermal stability as well as residual weight of the nanocomposites increases with the increase of the clay content. The formation of more residual weight after thermal decomposition may lead to the enhancement of overall thermal stability of the nanocomposites [32]. The 15 °C more increment

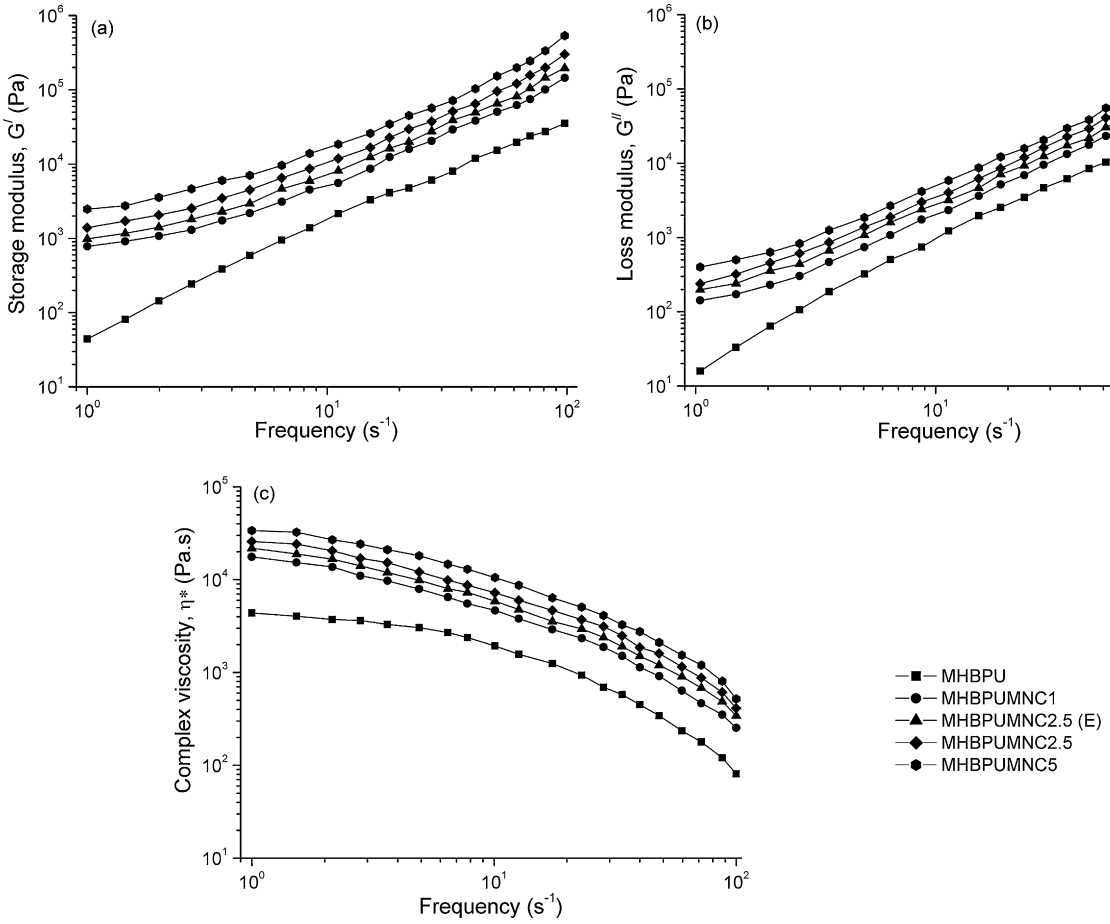

Fig. 7. Variation of (a) Storage modulus (G'), (b) Loss modulus (G'') and (c) Complex viscosity (η^*) of the pristine polymer and nanocomposites.

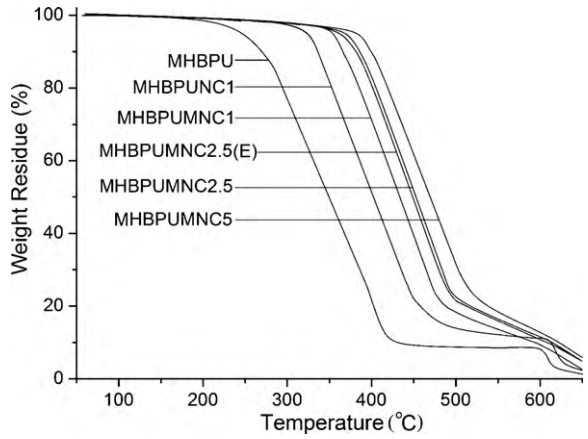

Fig. 8. TGA thermograms of the pristine polymer and nanocomposites.

of the decomposition temperature compared to earlier reported OMMT based nanocomposite, MHBPUNC2.5 [17] was attributed to the high thermostability of the s-triazine ring and the presence of nitrogen elements in the HBPAA [13]. Interestingly, while the MHBPU and MHBPUNC2.5 showed two step degradation patterns [15,17], the modified OMMT nanocomposites showed only one step degradation pattern (Fig. 8). This may be due to the incorporation of the s-triazine based HBPAA modified OMMT into the matrix system. The formation of more interactions between the modified OMMT and matrix (as obtained from FTIR study) increases the crosslinking density and thereby bridging the polymer backbones together (as shown in Scheme 1). This results the development of a "hard material" with restricted molecular mobility.

The thermal properties of the nanocomposites were also studied by DSC. The DSC thermograms of the nanocomposites are shown in Fig. 9. The melting temperature (T_m) of the nanocomposites was found to be increased from 50 °C to 58 °C (Table 2). The enhancement of the melting temperature is due to the formation of dense structure that is caused by the increase of different types of molecular interactions with nanoclay loading. Further the increase value of the melting enthalpy (ΔH_m) with the increase of clay content may result from the slight enhancement in the degree of crystallinity of the PCL moiety (Table 2). Here the exfoliated nanoclay is acting as a nucleating agent as this effect is well known [17]. This result is also well agreement with the observed XRD data.

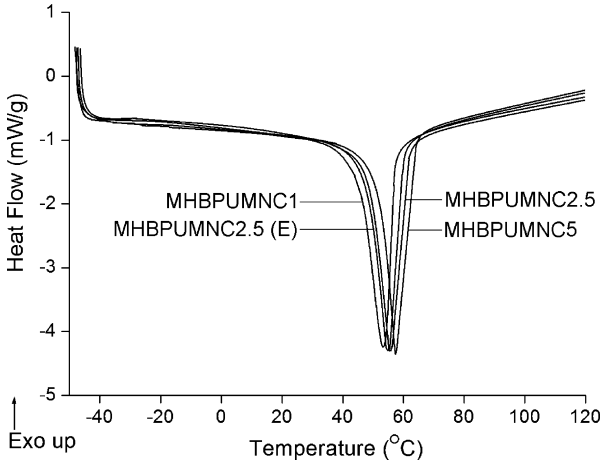

Fig. 9. DSC thermograms of the nanocomposites.

3.7. Flame retardancy of the nanocomposites

The flame retardancy of the prepared nanocomposites was examined by UL94 and LOI tests. According to the UL94 rating the MHBPU matrix and the nanocomposites can be categorized as V2 and V1 rating respectively (Table 1). The LOI test results are also given in Table 1. The improvement of the flame retardancy of polymer/clay nanocomposites was explained in several literatures [33,34]. During the combustion of the systems the organ modified clay forms a barrier layer. Upon heating the nanoclay layers can migrate and accumulate on the surface of the nanocomposites as the viscosity of the systems decreases with temperature. The protective layers prevent the diffusion heat and air to the material. Further, the migration of the clay layers are instigated by the formation of gas bubbles, initiated by the decomposition of both organo modifiers and the polymer chains. Moreover, the formed strong protonic catalytic sites on the surface of the nanocomposites on heating, can be catalyzed the formation of stable char residue. The char formation during the thermal degradation of the nanocomposites plays an important role in the improvement of the flame retardant behavior. The importance of modification of clay in improving the flame retardancy by formation of char residue was elucidated by Song et al. [35]. They explained the mechanism on the basis of Bronsted acid site on the modified OMMT surface. The insulative layers of char residue retards the heat and oxygen transfer to the nanocomposites to feed the flame [36]. The dispersion state of the clay layers is also crucial factor in determining the improvement of the flame retardancy [37]. The HBPAA modified OMMT can disperse homogeneously due to the higher interactions (as discussed earlier). This explained higher flame retardancy of MHBPUMNC2.5 nanocomposite than the MHBPUNC2.5 (Table 1). Thus the formation of continuous OMMT-rich carbonaceous surface is more capable of preventing combustion [35]. With the increase of clay content the effect was more, as obvious.

4. Conclusion

The present investigation shows the successful way of preparation of modified OMMT/bio-based MHBPU nanocomposites. The s-triazine ring containing highly branched poly(amido amine) was synthesized fruitfully by using an $A_2 + B_3$ technique. The formation of poly(amido amine) was well characterized with the help of different spectroscopic and analytical techniques. This polymer was further utilized to modify the OMMT. From the XRD analysis the sonication based modification was found to be more effective than the modified clay obtained by exchanged process and hence concentration dependence study was carried out by taking sonication modified clay. The well dispersed organo-nanoclay in the matrix can be revealed from the FTIR, XRD, SEM and TEM analyses. The effect of modification of OMMT on the properties like physical, mechanical, thermal and flame retardancy of the nanocomposites was elucidated extensively. As the modification helps in better distribution of the nanoclay in the matrix thus the improvements of most of the properties are sought-after. Further the biodegradability of these systems is under progress, which may show the potentiality of the materials as advanced biomaterials.

Acknowledgement

The authors express their thanks to the financial assistance of DST, India through the grant no. SR/S3/ME/13/2005-SERC-Engg, dated 9th April, 2007.

References

[1] R.S. Sinha, M. Okamoto, Prog. Polym. Sci. 28 (2003) 1539.

[2] S. Pavlidou, C.D. Papaspyrides, Prog. Polym. Sci. 33 (2008) 1119.
[3] N. Karak, J. Polym. Mater. 23 (2006) 1.
[4] C. Kaynak, G.I. Nakas, N.A. Isitman, Appl. Clay Sci. 46 (2009) 319.
[5] M. Huskic, E. Zagar, M. Zigon, I. Brnardic, J. Macan, M. Ivankovic, Appl. Clay Sci. 43 (2009) 420.
[6] P.K. Maji, P.K. Guchhait, A.K. Bhowmick, J. Mater. Sci. 44 (2009) 5861.
[7] L.B.d. Paiva, A.R. Morales, F.R.V. Diaz, Appl. Clay Sci. 42 (2008) 8.
[8] N.N. Herrera, J.M. Letoffe, J.L. Putaux, L. David, E. Bourgeat-Lami, Langmuir 20 (2004) 1564.
[9] K. Yoon, H. Sung, Y. Hwang, S.K. Noh, D. Lee, Appl. Clay Sci. 38 (2007) 1.
[10] T.D. Fornes, P.J. Yoon, D.L. Hunter, H. Keskkula, D.R. Paul, Polymer 43 (2002) 5915.
[11] J. Xiong, Z. Zheng, H. Jiang, S. Ye, X. Wang, Compos. Part A 38 (2007) 132.
[12] S.S. Mahapatra, N. Karak, J. Appl. Polym. Sci. 106 (2007) 95.
[13] S.S. Mahapatra, N. Karak, Polym. Degrad. Stabil. 92 (2007) 947.
[14] C. Hepburn, Polyurethane Elastomers, Elsevier Applied Science, London, 1992.
[15] H. Deka, N. Karak, J. Appl. Polym. Sci. 116 (2010) 106.
[16] H. Deka, N. Karak, Prog. Org. Coat. 66 (2009) 192.
[17] H. Deka, N. Karak, Nanoscale Res. Lett. 4 (2009) 758.
[18] J.W. Gilman, Appl. Clay Sci. 15 (1999) 31.
[19] P.S. Kalsi, Spectroscopy of Organic Compounds, New Age International Publishers, New Delhi, 2004.
[20] J. Borah, N. Karak, Polym. Int. 53 (2004) 2026.
[21] C.J. Hawker, R. Lee, J.M.J. Frechet, J. Am. Chem. Soc. 113 (1991) 4583.
[22] T. Uchida, A. Hamano, N. Kawashima, S. Takeuchi, Electron. Commun. Jpn. 90 (2007) 93.
[23] M. Modesti, A. Lorenzetti, D. Bon, S. Besco, Polymer 46 (2005) 10237.
[24] M.S. Kim, J.K. Jun, H.M. Jeong, Compos. Sci. Technol. 68 (2008) 1919.
[25] H.T. Lee, L.H. Lin, Macromolecules 39 (2006) 6133.
[26] S. Rana, N. Karak, J.W. Cho, Y.H. Kim, Nanotechnology 19 (2008) 495707.
[27] B. Sreedhar, D.K. Chattopadhyay, V. Swapna, J. Appl. Polym. Sci. 100 (2006) 2393.
[28] J. Ren, B.F. Casanueva, C.A. Mitchell, R. Krishnamoorti, Macromolecules 36 (2003) 4188.
[29] G. Galgali, C. Ramesh, A. Lele, Macromolecules 34 (2001) 852.
[30] S.R. Ha, S.H. Ryu, S.J. Park, K.Y. Rhee, Mater. Sci. Eng. A 448 (2007) 264.
[31] X. Kornmann, R. Thomann, R. Mulhaupt, J. Finter, L. Berglund, J. Appl. Polym. Sci. 86 (2002) 2643.
[32] J.H. Park, H.M. Lee, I.J. Chin, H.J. Choi, H.K. Kim, W.G. Kang, J. Phys. Chem. Solid 69 (2008) 1375.
[33] M. Lewin, Polym. Adv. Technol. 17 (2006) 758.
[34] J. Xiong, Y. Liu, X. Yang, X. Wang, Polym. Degrad. Stabil. 86 (2004) 549.
[35] R. Song, Z. Wang, X. Meng, B. Zhang, T. Tang, J. Appl. Polym. Sci. 106 (2007) 3488.
[36] M. Zanetti, T. Kashiwagi, L. Falqui, G. Camino, Chem. Mater. 14 (2002) 881.
[37] H.O. Pastore, A. Franche, E. Boccaleri, L. Marchese, G. Camino, Macromol. Mater. Eng. 289 (2004) 783.